12. Bochkarev M N, Vitukhnovsky A G, Katkova M A *Organicheskie Svetoizluchayushchie Diody* (*OLED*) (Organic Light-Emitting Diodes (OLEDs)) (Nizhny Novgorod: DEKOM, 2011)
13. Tu C-C et al. *Appl. Phys. Lett.* **98** 213102 (2011)
14. Cheng K-Y et al. *Nano Lett.* **11** 1952 (2011)
15. Vasiliev R B, Dirin D N, Gaskov A M *Russ. Chem. Rev.* **80** 1139 (2011) [*Usp. Khim.* **80** 1190 (2011)]
16. Anikeeva P O et al. *Nano Lett.* **9** 2532 (2009)
17. Wood V et al. *Nano Lett.* **9** 2367 (2009)
18. Vashchenko A A et al. *JETP Lett.* **96** 113 (2012) [*Pis'ma Zh. Eksp. Teor. Fiz.* **96** 118 (2012)]
19. Förster Th *Ann. Physik* **437** 55 (1948)

PACS numbers: 72.80.Le, 72.80.Tm, 73.40.Lq, 73.61.Le, 73.61.Ph
DOI: 10.3367/UFNe.0183.201306i.0657

Organic optoelectronics based on polymer–inorganic nanoparticle composite materials

A N Aleshin

Nanocomposite materials based on conducting polymers and inorganic nanoparticles are of great interest due to their practical applications in organic electronic devices such as organic light-emitting diodes (OLEDs), organic field-effect transistors (OFETs), solar batteries, and memory cells [1–5]. Elements of organic electronics based on polymer–inorganic nanoparticle hybrid materials are compatible with printing organic electronics technology, which is currently one of the most promising due to its high efficiency and low net cost.

The integration of organic materials (polymers) and inorganic materials (nanoparticles) at the nanolevel can be used to manufacture optoelectronic structures combining 3D polymer matrix technology with the unique electric and optical properties of inorganic nanoparticles (0D quantum dots $\sim$ 10 nm in size). Both components operate together in such structures, providing control of the radiation color emitted by OLEDs. The emission spectrum depends on the polymer type and the type, size, and functioning of nanoparticles. In particular, to obtain white emission, materials emitting in the blue, green, and red (or blue and orange) spectral regions must be combined in one structure. The combination of emitters operating in different spectral regions requires understanding and controlling charge-carrier transfer processes in such systems, where the exciton transport from a wide-band (blue) emitter to a narrow-band (orange, red) emitter can lead to emission of light only from the narrow-band material for a 100% energy transfer efficiency.

The control of charge transfer processes for achieving the successive emission of light from all materials contained in the active layer of an OLED is the most important problem for obtaining white emission. This problem can be resolved by combining the optimal selection of emitting components in the active layer, their relative concentrations, and the possibility of controlling their interaction at the molecular level.

A N Aleshin Ioffe Physical Technical Institute, Russian Academy of Sciences, St. Petersburg, Russian Federation
E-mail: aleshin@transport.ioffe.ru

Uspekhi Fizicheskikh Nauk **183** (6) 657 – 664 (2013)
DOI: 10.3367/UFNr.0183.201306i.0657
Translated by M Sapozhnikov; edited by A M Semikhatov

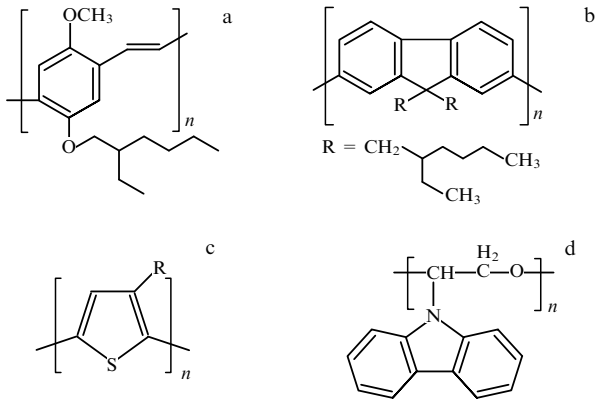

Figure 1. Molecular structure of semiconductor polymers used in organic electronic devices: (a) MEH-PPV ($E_g \approx 2.34$ eV); (b) PFO ($E_g \approx 2.9$ eV); (c) P3HT ($E_g \approx 2.0$ eV); (d) PVC ($E_g \approx 3.6$ eV).

One of the promising ways for manufacturing low-cost, large-area white OLEDs deposited from solution onto substrates by jet printing methods is the combination of several emitting materials in one active layer. This approach uses the mixing of two or three polymers in the active layer, which emit in different spectral regions, thereby controlling the emission color, or doping a wide-band material with a narrow-band material, the wide-band material being a medium for the charge carrier transfer. Important in this field are the development of white OLEds based on a polymer mixture [6, 7] and the creation of polymer–inorganic nanoparticle hybrid active layers for white OLEDs [2]. Recently, we investigated the properties of the polymer–inorganic nanoparticle hybrid active layers that we obtained for white OLEDs [8–12] and OLEDs based on polymers doped with polymer nanoparticles [13] emitting in different spectral ranges, from UV to IR.

The polymers that we studied (derivatives of polyphenylene vinylene (PPV), polyfluorene (PFO), polyvinylcarbazole (PVC), etc.), with the structural formulas shown in Fig. 1, are soluble in usual organic solvents, while inorganic semiconductor particles (ZnO, Si, CdS, CdSe, etc.) deposited from solutions had diameters of 10–50 nm and the band gap E_g from ≈ 1.8 eV (Si) to ≈ 3.35 eV (ZnO). This opens up possibilities for the deposition of composites from solutions on both ordinary glass substrates and flexible substrates using jet printer technology. The parameters of OLEDs based on multilayer composite structures are expected to be higher than these of purely polymer OLEDs due to the efficient radiative recombination in both the polymer and nanoparticles, and also in their complexes [2]. An important advantage of composite OLED structures is that the characteristic relaxation times of charge carriers in them are considerably shorter (by two–three orders of magnitude) than those in structures based on liquid crystals, while the doping of a polymer matrix with inorganic nanoparticles slows down the degradation of a hybrid structure, thereby increasing the life of such devices.

As shown in [8–12], the use of composite active layers in OLEDs based on semiconductor conjugated polymers and

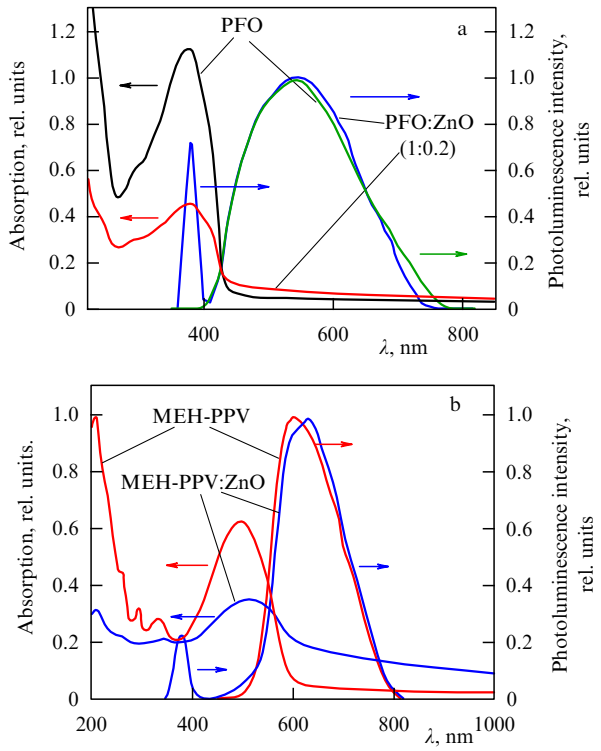

Figure 2. Absorption and photoluminescence spectra of (a) PFO and PFO:ZnO films (1.0:0.2); and (b) MEH-PPV and MEH-PPV:ZnO (2:1) films.

semiconductor inorganic nanoparticles opens up new possibilities for controlling the emission color of active layers. The emission color of the composite active layer of an OLED can be controlled by several methods:

(i) selecting the polymer type and the kind of nanoparticles;

(ii) changing the concentration ratio for a polymer and nanoparticles in a composite;

(iii) changing the size and functioning of nanoparticles;

(iv) applying an external electric field.

In the first case, the use of PPV derivatives can give a red, green, and even blue emission color, PFO derivatives provide green and blue emission colors, while PVC derivatives emit blue light. The use of semiconductor nanoparticles in composites provides emission in a broad range from red (Si) to blue (ZnO) spectral regions.

Figure 2 shows typical absorption and photoluminescence spectra of PFO films and a PFO:ZnO (1.0:0.2) composite (Fig. 2a) and MEH-PPV and MEH-PPV:ZnO (2:1) (Fig. 2b). We can see from Fig. 2a that the absorption spectra of a PFO film and a composite PFO:ZnO film (the ZnO concentration is ≈ 17 wt.%, 1:0.2) exhibit maxima at $\lambda \approx 380$ nm; however, the intensity of this maximum for the hybrid film is lower and a weak absorption band is observed at $\lambda > 430$ nm. This means that the doping of a polymer matrix with ZnO nanoparticles reduces absorption in such a composite film, which therefore becomes more transparent. This fact confirms the presence of interaction between polymer molecules and inorganic nanoparticles. The luminescence spectra of PFO and PFO:ZnO films for different polymer–ZnO nanoparticle concentration ratios (1:0.2 and 1:1) obtained in [12] show that the doping of PFO with ZnO particles leads to a blue shift of the 580 nm luminescence band. As the concentration of ZnO nanoparticles increases, the intensity of the 380 nm luminescence band related to ZnO nanoparticles increases, while the intensity of the 580 nm band related to PFO decreases. By changing the polymer-to-nanoparticle concentration ratio in hybrid PFO:ZnO films, we can obtain green (pure PFO and 1:0.2) and white (PFO:ZnO, 1:1) emission [12].

A similar picture is also observed for another optically active polymer, MEH-PPV, and its composites MEH-PPV:ZnO (the concentration of ZnO nanoparticles is ≈ 33 wt.% and the weight polymer-to-nanoparticle ratio is 2:1). It follows from Fig. 2b that the absorption spectra of MEH-PPV films and composite MEH-PPV:ZnO films have maxima at $\lambda \approx 500$ nm. As in the case of PFO:ZnO, the doping of a MEH-PPV polymer with ZnO nanoparticles reduces absorption in the composite film compared to that in the MEH-PPV film, which again confirms the presence of interaction between MEH-PPV polymer molecules and ZnO nanoparticles. The luminescence spectra of MEH-PPV and MEH-PPV:ZnO films presented in Fig. 2b show that ZnO nanoparticle doping of the polymer matrix causes the red shift of the luminescence band from $\lambda \approx 600$ nm (MEH-PPV) to $\lambda \approx 640$ nm (MEH-PPV:ZnO). As the concentration of ZnO nanoparticles increases, the 380 nm luminescence band related to ZnO nanoparticles appears [19].

The characteristic relaxation times of excited states in MEH-PPV and MEH-PPV:ZnO (ZnO ≈ 33 wt.%) films were estimated from the photoluminescence kinetics of these films using the relation $I_{\mathrm{PL}} \sim \exp(-t/\tau)$ for the luminescence intensity, where τ is the excited-state lifetime. It was found that the excited-state lifetime of MEH-PPV measured at the maximum of the 650 nm luminescence band was ≈ 2.5 ms, which is 1.4 times longer than the lifetime of carriers, ≈ 1.8 ms, in a composite MEH-PPV:ZnO film measured at the maximum of the 650 nm luminescence band. Hence, the excited-state lifetime in a pure MEH-PPV film decreases after doping this film with ZnO nanoparticles, which indicates an increase in the concentration of defects in a polymer MEH-PPV chain [11].

Studies of luminescence spectra of composite films based on MEH-PPV and PFO derivatives and ZnO nanoparticles have shown general properties inherent in these systems, which have two bands in the blue (ZnO) and green–red (polymer) spectral regions. As the concentration of ZnO nanoparticles increased, luminescence bands shifted to the UV region, and 'concentration' quenching of polymer luminescence was observed, which allows modulating the luminescence wavelength between different ranges in the visible region and obtaining white emission for certain ratios of components in the composite [9, 11, 12]. Luminescence spectra observed in experiments suggest that the charge transfer occurs between the polymer matrix and ZnO nanoparticles, and charge transfer complexes are formed. The simultaneous combined emission of both components of the composite is provided by a partial suppression of energy transfer from ZnO nanoparticles emitting in the blue range to PFO and MEH-PPV polymers emitting in the green–orange–red range [9, 11, 12].

The current–voltage characteristic ('IV') of composite MEH-PPV:ZnO films obeys the power law $I(V) \propto V^{\beta}$ with three different exponents: $\beta \approx 1$, $\beta \approx 2.5-3.0$, and $\beta \approx 1.5$. The IV asymmetry, nonlinearity, and power law resemble the transport mechanism determined by currents restricted by a spatial charge. The type of current relaxation with time

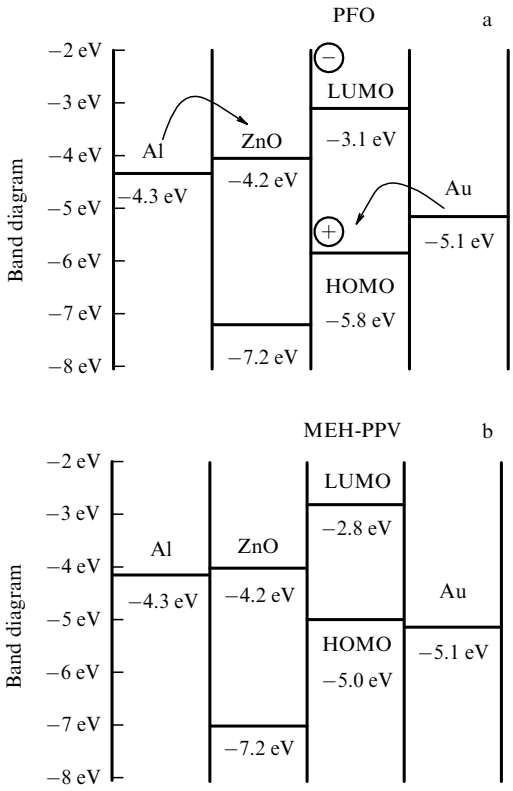

Figure 3. Band diagrams of (a) Au–PFO:ZnO–Al and (b) Au–MEH-PPV:ZnO–Al structures.

depends on the voltage applied and is determined by the transition of carriers to localized states [9].

As shown in [8, 9, 11], for a certain concentration ratio of a polymer (PPV derivatives) and ZnO nanoparticles, it is possible to modulate the luminescence wavelength between red and green emission [8, 9] and also between light-blue and dark-blue colors [11] by applying a planar electric field to the composite active layer of this OLED. This effect in composite films based on the PPV copolymer and ZnO nanoparticles is manifested in the suppression of the polymer emission in the green spectral region in an electric field with a strength above 2×10^4 V cm^{-1}, which is related to the electric-field-dependent excimer luminescence and the electric-field-induced dissociation of complexes based on the aromatic components of the copolymer and ZnO particles [9]. It was found in [9, 11] that exciplex states connecting charge carriers in a polymer matrix and inorganic nanoparticles were formed in composite films based on PPV copolymers and ZnO nanoparticles. This effect opens up the door to modulating the OLED emission color by a planar electric field, which considerably simplifies the manufacturing technology of polymer OLEDs.

Figure 3 presents band diagrams of Au–PFO:ZnO–Al and Au–MEH-PPV:ZnO–Al structures studied in [11, 12]. We see that the mechanism of formation of excited states in a polymer–nanoparticle structure assumes the presence of several radiative recombination channels and efficient charge transfer between components of the composites [8–12]:

(i) excitation of carriers on the highest occupied molecular orbital (HOMO) and their transition to the lowest unoccupied molecular orbital (LUMO) in a polymer (MEH-PPV, PFO, etc.) followed by their recombination, including the exciton channel;

(ii) band–band recombination in ZnO nanoparticles, including impurity levels;

(iii) formation of polymer–nanoparticle complexes, including excited states at the polymer–nanoparticle (exciplex) interface.

Recombination involving exciplex states in composite polymer–ZnO nanoparticle films assumes the capture of carriers due to tunneling injection and the participation of exciplex states (without a barrier). The latter mechanism includes the capture of carriers and formation of an 'exciplex' state and radiative charge-transfer 'exciplex'–complex recombination, which can be controlled by a planar electric field.

The parameters of exciplex states in composite MEH-PPV:ZnO films (10 wt.% of ZnO) were estimated from the photoluminescence kinetics formula $I_{\mathrm{PL}} \sim \exp(-t/\tau)$, where τ is the lifetime of the carriers. It was found that the lifetime τ ($\sim$ 164 ns) for exciplex states for $\lambda \approx 420$ nm was approximately six times longer than for the components of the composite: ZnO ($\sim$ 29 ns for $\lambda \approx 380$ nm) and MEH-PPV ($\sim$ 24 ns for $\lambda \approx 630$ nm), which proves the formation of exciplex states in composite films based on semiconductor polymers and inorganic nanoparticles [11].

A new area of studies in the field of organic electronics is the development of light-emitting organic field-effect transistors (LE-OFETs), combining emission properties of OLEDs with switchable properties of OFETs [14]. The specific features of LE-OFETs are that they can operate in both the unipolar [14, 15] and ambipolar [16–18] regimes; they are characterized by the presence of an electron–hole (p−n) transition controlled by a voltage across a gate, and they emit light from the overlap band of injected carriers. The LE-OFET structure illustrating the injection of electrons and holes from a source and a drain in the ambipolar regime is shown in Fig. 4.

Recent studies have demonstrated LE-OFETs with active layers consisting of monopolymers [14–18], polymer mixtures [19], two-polymer [20] or three-polymer [21] layers. The emission efficiency of a three-layer LE-OFET proved to be comparable to that of equivalent OLEDs or even exceeded it [21]. However, before our studies, no information was available in the literature on LE-OFETs based on nanocomposite materials containing semiconductor polymers and inorganic nanoparticles.

We recently demonstrated [22–24] LE-OFETs with composite active layers based on soluble PFO and MEH-PPV polymers used as matrices and semiconductor ZnO nanoparticles. PFO is a promising stable polymer for the active layers of green OLEDs, while MEH-PPV is widely used in orange OLEDs in polymer optoelectronics. The structural formulas of these molecules are shown in Fig. 1. As an inorganic component, we used nanoparticles of ZnO, which is a nontoxic transparent inorganic semiconductor with a high mobility of charge carriers, up to 20 cm^2 V^{-1} s^{-1}. An important feature of our LE-OFET structures is asymmetric Al and Au electrodes for the injection of electrons and holes into ZnO and PFO (MEH-PPV), respectively. The band diagrams of Au–PFO:ZnO–Al and Au–MEH-PPV:ZnO–Al structures for composite LE-OFETs are shown in Fig. 3. We manufactured and studied OFETs based on composite PFO:ZnO and MEH-PPV:ZnO films with the concentration of ZnO nanoparticles ranging from $\approx$ 17 to 50 wt.% (i.e.,

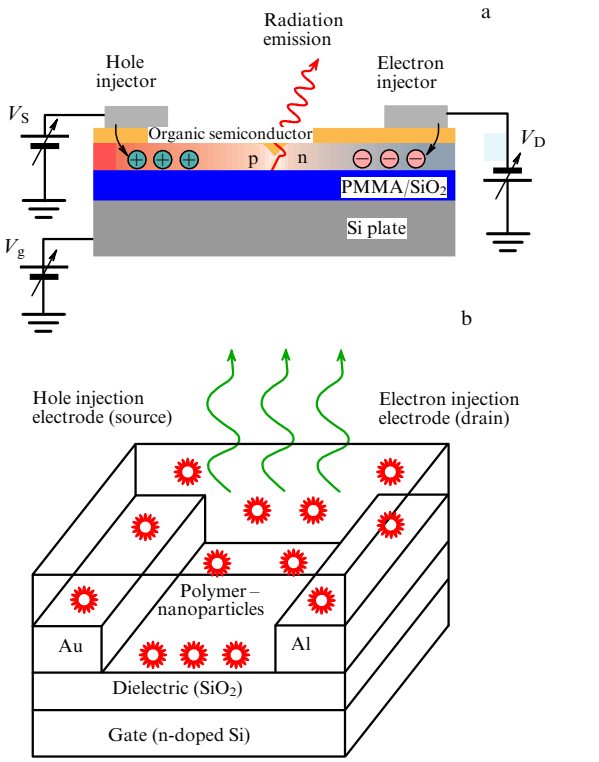

Figure 4. (a) Conceptual schematic of the LE-OFET operation; V_S, V_g, and V_D are the respective source, gate, and drain voltages. PMMA: polymethyl methacrylate. (b) LE-OFET structure based on a PFO:ZnO film.

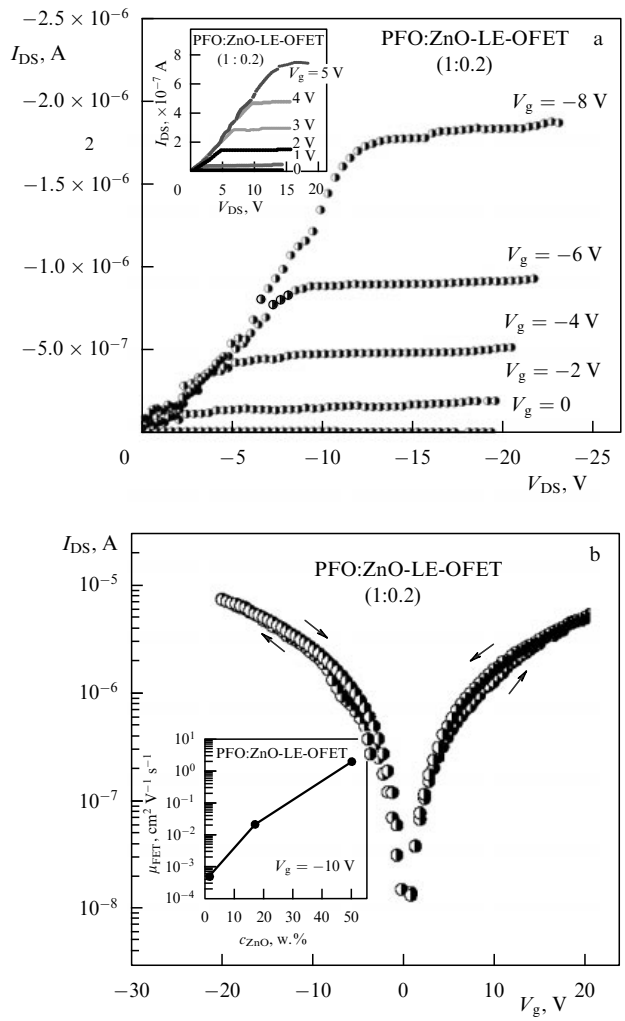

Figure 5. (a) Current–voltage characteristic of a PFO:ZnO (1:0.2)-OFET for different negative values of V_g. The inset shows the IV of the same sample for different positive values of V_g. (b) Transient characteristics of a PFO:ZnO (1:0.2)-OFET for $V_{DS} = -10$ V. The inset shows the dependence of the mobility of charge carriers in the PFO:ZnO-OFET on the concentration c_{ZnO} of ZnO nanoparticles.

from 1:0.2 to 1:1). It was shown that OFET structures based on composite PFO:ZnO and MEH-PPV:ZnO films for different relations between components can operate in both unipolar and ambipolar regimes [22–24].

Figure 5a shows typical IVs of an OFET based on a composite PFO:ZnO (1:0.2) film obtained in a vacuum for different voltages V_g across the gate. We can see from this figure that the behavior of these IVs for negative V_g is typical for hole transport in the regime close to saturation. The dependences of I_{DS} on V_{DS} are not completely flat, which is probably explained by the influence of the leakage current between the electrodes (the source and the gate). At sufficiently high voltages $V_{DS} > 25$ V between the drain and source, a sharp increase in I_{DS} was observed for the OFET based on PFO:ZnO films, which is consistent with the behavior of IVs observed previously for OFETs based on other organic materials [15, 24]. Such superlinear IVs indicate the appearance of a channel related to electron transport at negative values of V_g. For positive V_g, the IV behavior was similar, as is shown in the inset in Fig. 5a, which is consistent with the results of numerical simulation [25] predicting a superlinear increase in the saturation current in the ambipolar regime of an OFET. The transient OFET characteristics in the saturation regime for positive and negative V_g are shown in Fig. 5b. The value of V_g was changed from 20 V to -20 V with a step of 0.5 V at the constant voltage $V_{DS} = -10$ V. We see from this figure that when the concentration of ZnO nanoparticles is relatively low (1:0.2), the PFO:ZnO-OFET operates in the accumulation regime, for both electrons and holes. In this case, the PFO:ZnO-OFET demonstrates transient characteristics with a small irreversible hysteresis with an amplitude that is considerably smaller than the hysteresis amplitude observed previously in the OFET based on pure PFO, which should improve the electric characteristics of the composite OFET.

The mobility μ_{FET} of charge carriers of the composite active layer was estimated from the OFET IV in the saturation and weak-field regimes from the relations [26]

$$I_{DS} = \frac{W}{2L}\,\mu_{FET} C_I (V_g - V_{th})^2\,, \qquad (1)$$

$$I_{DS} = \frac{W}{L}\,\mu_{FET} C_I (V_g - V_{th}) V_{DS}\,, \qquad (2)$$

where W is the channel width, L is the channel length, C_I is the capacitance per SiO_2 unit area (for the thickness ≈ 200 nm, $C_I \sim 7-10$ nF cm^{-2}), V_g is the gate voltage, and V_{th} is the threshold voltage corresponding to the beginning of the accumulation regime.

The electron and hole mobilities μ_{FET} for PFO:ZnO-OFET were calculated from relations (1) and (2) for the respective saturation and weak-field regimes. For the OFET based on the PFO:ZnO (1:0.2) film with the IVs shown in Fig. 5, the electron and hole mobilities at 300 K calculated

from (1) were respectively ~ 0.021 and ~ 0.029 cm^2 V^{-1} s^{-1}. The on/off ratio characterizing the ratio of currents through the OFET without and with the gate bias, determined from transient characteristics, was $\sim 10^3$ for $V_g \approx -20$ V. This behavior of the IV and transient characteristics was also observed for other OFETs based on PFO:ZnO composite films with the concentration of ZnO nanoparticles from 10 to ≈ 50 wt.%. In this case, the mobility of carriers dramatically increased upon increasing the concentration of ZnO nanoparticles and reached $\mu_{FET} \approx 2$ cm^2 V^{-1} s^{-1} for PFO:ZnO-OFET (1:1) (the inset in Fig. 5b).

The relatively low values of V_{th} and on/off ratio observed in experiments indicate a low concentration of states related to traps and low injection barriers in contacts. The values of μ_{FET} obtained in our experiments at 300 K for the PFO:ZnO-OFET with an intermediate concentration of ZnO nanoparticles are much higher than those that are usually observed for OFETs based on pure PFO films, which can be related to the contribution of the p- and n-components of the PFO:ZnO composite to the charge transfer process. We also obtained high electron and hole mobilities at 300 K for OFETs based on MEH-PPV:ZnO (2:1) films, which were ≈ 1.2 and ≈ 1.4 cm^2 V^{-1} s^{-1}, respectively [24]. The on/off ratio for this OFET was $\approx 10^4$ for $V_g \approx -30$ V, which is even higher than these ratios obtained for PFO:ZnO-OFET [22, 23]. The high values of μ_{FET} ($T = 300$ K) obtained for the OFET based on composite PFO:ZnO and MEH-PPV:ZnO films can be related, in our opinion, to the contribution of the mobility of ZnO nanoparticles to the total mobility. Doping with ZnO nanoparticles can reduce the density of traps in a polymer and lead to the formation of ZnO–PFO and ZnO–MEH-PPV complexes and agglomerates between Al and Au electrodes. This explanation is confirmed by the high values of μ_{FET} ($T = 300$ K) obtained for polycrystalline ZnO (≈ 20 cm^2 V^{-1} s^{-1}) [27] and for the OFET based on ZnO (≈ 7.2 cm^2 V^{-1} s^{-1}) [28].

Figure 6a shows the optical output characteristics (the dependence of the electroluminescence (EL) intensity on V_{DS}) of an ambipolar LE-OFET based on PFO:ZnO (1:0.2) for negative and positive values of V_g. We see that the integrated EL intensity at 300 K increases with increasing the voltage V_{DS} for both negative and positive V_g. The dependence of the integrated LE intensity on V_{DS} in LE-OFETs based on composite PFO:ZnO films has a symmetric form. There is a fixed voltage $V_{DS} \approx 5$ V of the beginning of EL, which is independent of the concentration of ZnO nanoparticles and the polarity of V_g. This cut-off voltage can be observed for voltages V_g up to -30 V (Fig. 6a). This behavior of the dependence of the integrated EL intensity on V_{DS} is consistent with that observed for LE-OFETs based on tetracene, polyfluorene, and MEH-PPV:ZnO [14, 22–24]. However, in the case of the LE-OFET based on PFO:ZnO films, the cut-off voltage V_{DS} is half the voltage of LE-OFETs based on MEH-PPV:ZnO films.

The dependence of the integrated EL intensity on the electric field strength (up to $\approx 2.5 \times 10^3$ V cm^{-1}) was also measured for LE-OFETs based on PFO:ZnO and MEH-PPV:ZnO in different spectral ranges: (i) integrated; (ii) $\lambda \approx 600-830$ nm; (iii) $\lambda \approx 450$–620 nm; and (iv) $\lambda \approx 300$–400 nm. The EL spectrum of the LE-OFET based on PFO:ZnO is in the green spectral range, while the EL spectrum of the LE-OFET based on MEH-PPV:ZnO is in the red spectral range, which corresponds to the emission of the PFO polymer

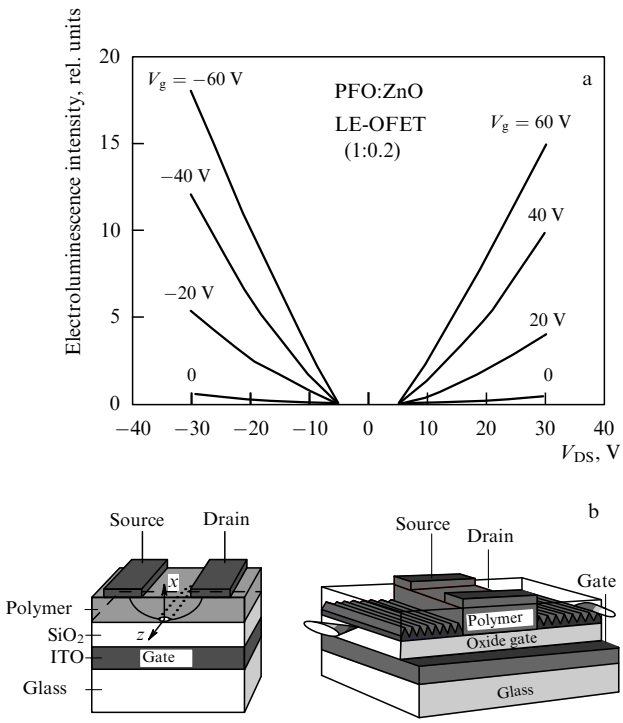

Figure 6. (a) Optical output characteristics of a PFO:ZnO (1:0.2)-LE-OFET: the integrated electroluminescence intensity as a function of V_{DS} for different V_g. (b) Design of an LE-OFET polymer injection laser (not yet realized in practice). ITO: indium tin oxide.

matrix and the emission of MEH-PPV and correlates with the photoluminescence spectrum of these composite films. The mechanism of the formation of excited states in composite PFO:ZnO and MEH-PPV:ZnO films includes the excitation of carriers to the HOMO followed by their transition to the LUMO in PFO and MEH-PPV polymers and their recombination, the contribution of emission from ZnO nanoparticles (at $\lambda \approx 380$ nm) to the radiative recombination, and the contribution of emission from polymer–nanoparticle complexes. As shown in [11], some recombination channels in such systems can be suppressed by varying the concentration of ZnO nanoparticles.

An analysis of the band diagrams of Au–PFO:ZnO–Al and Au–MEH-PPV:ZnO–Al presented in Fig. 3 shows that the respective work functions for Au and Al electrodes in the case of Au–MEH-PPV:ZnO–Al are ≈ 5.1 and ≈ 4.3 eV, whereas the respective HOMO and LUMO energies in MEH-PPV are ≈ 5.0 and ≈ 2.8 eV. Therefore, the barrier for holes in the Au–MEH-PPV contact is ≈ 0.1 eV, and for electrons in the Al–MEH-PPV contact is ≈ 1.5 eV. This makes the Au contact preferable for the injection of holes into an MEH-PPV polymer. On the other hand, energies corresponding to the edges of the valence band (≈ 7.5 eV) and conduction band (≈ 4.2 eV) in ZnO clearly indicate the presence of a high energy barrier for holes, which, however, can be overcome during the transport of carriers from ZnO to MEH-PPV; in this case, the injection barrier energy for electrons in the Al–ZnO contact is ≈ 0.1 eV. It follows from the values presented above that the Au–MEH-PPV:ZnO–Al structure should work as an ambipolar LE-OFET, which is consistent with our experimental results for LE-OFETs based on MEH-PPV:ZnO films with a relatively low concentration of ZnO nanoparticles. Similar results were obtained for LE-OFETs based on PFO:ZnO films. We can

assume that doping with ZnO nanoparticles reduces the density of traps in MEH-PPV and PFO polymers, which increases the mobility in such OFETs.

According to the emission mechanism of LE-OFET structures proposed in [29, 30], emission in the unipolar regime is caused by the presence of a stable electron reservoir in a polymer in the vicinity of the Al contact. The transport of charge carriers in the Al–MEH-PPV structure (Al–PFO) occurs after the formation of the contact and the appearance of a constant electrochemical potential in it. The diffusion of electrons from the metal to MEH-PPV (PFO) ceases after the appearance of the electric field self-induced by the accumulated charge, the excessive electrons being concentrated near the Al contact. In the accumulation regime, holes move from the source, the Au electrode, to the drain, the Al electrode, on which they can be either absorbed by the metal or recombine with electrons in the reservoir, the volume charge. It was shown recently that the transition from the unipolar transport regime to the ambipolar regime leads to a change in the position of the recombination region of charge carriers during the motion of carriers from one contact to another [18, 29, 30]. The recombination of charge carriers in the ambipolar regime most likely occurs at the polymer–dielectric and polymer–ZnO nanoparticle interfaces, rather than in the contacts. The recombination region can move from the metal–polymer interface to the polymer–dielectric and polymer–ZnO nanoparticles interface, which leads to the transition from the unipolar transport regime to the ambipolar regime. In this case, spatial inhomogeneities of channels in LE-OFETs based on MEH-PPV:ZnO and PFO:ZnO can affect EL and the injection of electrons and holes from Al and Au electrodes.

At present, polymer and composite LE-OFETs are used for illumination of OLED panels (LE-OFETs based on F8BT films [31]) and for manufacturing active light-emitting arrays based on Alq3-LE-OFET containing 16×16 linear pixel arrays [32]. In the latter case, LE-OFETs replace equivalent OLEDs. Importantly, LE-OFETs based on soluble conjugated polymers and semiconductor nanoparticles are multifunctional devices, not only operating as OLEDs and OFETs but also showing promise for applications in logical elements and elements of resistive and OFET memory based on composites [33], whose manufacturing technology is compatible with modern printing organic electronic technologies. Polymer and composite films are promising for applications in composite solar batteries [34] and organic wires for connecting elements [35]. At the same time, these devices offer many possibilities due to a number of unique features of polymer LE-OFETs:

(i) the high gate-voltage-induced density of charge carriers implying the inverse population of levels;

(ii) minimal losses on the source and drain electrodes;

(iii) minimal gate losses (Si- or ITO-doped gate);

(iv) restriction of the electron–hole recombination region in the ambipolar regime of an LE-OFET by a narrow band near a dielectric located far from the electrodes.

All these factors allow the development of an injection laser based on polymer and composite LE-OFETs, whose design is described in [36] (Fig. 6b). All the avenues of study discussed above are important elements of modern printing organic electronics, in particular, the manufacturing technology of thin polymer screens, solar batteries, etc., by jet printing, roll-to-roll printing, and stamping. The technology of composite OLEDs and LE-OFETs can be easily incorporated into the already existing technology lines for manufacturing polymer devices.

Acknowledgments

This work was supported by the program P-8 of fundamental studies of the RAS Presidium in the area of Polyfunctional Materials for Molecular Electronics and by the Russian Foundation for Basic Research (grant no. 11-02-00451-a).

References

1. Skotheim T A, Reynolds J R (Eds) *Handbook of Conducting Polymers. Conjugated Polymers. Processing and Applications* 3rd ed. (Boca Raton: CRC Press, 2007); *Handbook of Conducting Polymers. Conjugated Polymers. Theory, Synthesis, Properties, and Characterization* 3rd ed. (Boca Raton: CRC Press, 2007)
2. Sessolo M, Bolink H J *Adv. Mater.* **23** 1829 (2011)
3. Sanchez C et al. *J. Mater. Chem.* **15** 3559 (2005)
4. Beek W J E, Wienk M M, Janssen R A J *Adv. Mater.* **16** 1009 (2004)
5. Sirringhaus H, Tessler N, Friend R H *Science* **280** 1741 (1998)
6. Alam M M, Jenekhe S A *Macromol. Rapid Commun.* **27** 2053 (2006)
7. Huang J et al. *Adv. Mater.* **18** 114 (2006)
8. Panin G N et al. *Appl. Phys. Lett.* **86** 113114 (2005)
9. Aleshin A N et al. *Solid State Commun.* **146** 161 (2008)
10. Aleshin A N, Alexandrova E L, Shcherbakov I P *Phys. Solid State* **50** 972 (2008) [*Fiz. Tverd. Tela* **50** 931 (2008)]
11. Aleshin A N, Alexandrova E L, Shcherbakov I P *J. Phys. D Appl. Phys.* **42** 105108 (2009)
12. Aleshin A N, Alexandrova E L, Shcherbakov I P *Eur. Phys. J. Appl. Phys.* **51** 33202 (2010)
13. Aleshin A N et al. *Phys. Solid State* **55** 675 (2013) [*Fiz. Tverd. Tela* **55** 617 (2013)]
14. Hepp A et al. *Phys. Rev. Lett.* **91** 157406 (2003)
15. Cicoira F et al. *Adv. Mater.* **18** 169 (2006)
16. Reynaert J et al. *J. Appl. Phys.* **97** 114501 (2005)
17. Swensen J S, Soci C, Heeger A J *Appl. Phys. Lett.* **87** 253511 (2005)
18. Zaumseil J et al. *Adv. Mater.* **18** 2708 (2006)
19. Loi M A et al. *Adv. Func. Mater.* **16** 41 (2006)
20. Dinelli F et al. *Adv. Mater.* **18** 1416 (2006)
21. Capelli R et al. *Nature Mater.* **9** 496 (2010)
22. Aleshin A N, Shcherbakov I P *J. Phys. D Appl. Phys.* **43** 315104 (2010)
23. Aleshin A N et al. *Organic Electron.* **12** 1285 (2011)
24. Aleshin A N et al. *Phys. Solid State* **54** 2508 (2012) [*Fiz. Tverd. Tela* **54** 2388 (2012)]
25. Verlaak S et al. *Appl. Phys. Lett.* **85** 2405 (2004)
26. Dimitrakopoulos C D, Malenfant P R L *Adv. Mater.* **14** 99 (2002)
27. Wang R, King L L H, Sleight A W *J. Mater. Res.* **11** 1659 (1996)
28. Pal B N et al. *Adv. Func. Mater.* **18** 1832 (2008)
29. Felmeier E J et al. *Adv. Mater.* **22** 3568 (2010)
30. Schidlej M et al. *Appl. Phys. Lett.* **95** 113303 (2009)
31. Cornil J et al. *Adv. Mater.* **19** 1791 (2007)
32. Cicoira F, Santato C *Adv. Func. Mater.* **17** 3421 (2007)
33. Aleshin A N, Fedichkin F S, Gusakov P E *Phys. Solid State* **53** 2370 (2011) [*Fiz. Tverd. Tela* **53** 2251 (2011)]
34. Aleshin A N *Innovatsii* (7) 96 (2012)
35. Aleshin A N *Adv. Mater.* **18** 17 (2006)
36. Heeger A J et al., US Patent No. 6828583